

Bearing health monitoring using optical fiber sensors

Shlomi Konforty¹, Michael Khmelnsky², Iddo Kressel³, Renata Klein⁴, Moshe Tur⁵ and Jacob Bortman⁶

^{1,2,6} PHM Lab, Department of Mechanical Engineering, Ben-Gurion University of the Negev, P.O. Box 653, Beer Sheva 84105, Israel

shlomiko@post.bgu.ac.il

mikelmh2@gmail.com

jacbort@bgu.ac.il³ Israel Aerospace Industries, Israel

ikressel@iai.co.il

⁴ R.K. Diagnostics, Gilon, P.O.B. 101, D.N. Misgav 20103, Israel

renata.klein@rkdiagnostics.co.il

⁵ School of Electrical Engineering, Tel Aviv University, Ramat Aviv 69978, Israel

tur@eng.tau.ac.il

ABSTRACT

Bearings are vital elements in rotating machinery. Failures in bearings can result in irreversible damage. Therefore, early detection of bearing damage and monitoring of fault severity are necessary for optimization of maintenance decisions.

The classical methods for bearing monitoring are based on analysis of vibration signals captured by accelerometers, usually located on the machine case. Two difficulties arise when diagnosing bearings in that manner. The first difficulty is the distortion of the signals due to the transmission path to the sensor. The second difficulty is the characteristic low signal to noise ratio, resulting from the weak bearing signals in the presence of the strong surrounding noise, originating from the vibrations of other rotating components in the machine.

The goal of the present study was to research the possibility of using an optical fiber sensor of the Fiber Bragg Grating (FBG) type, which senses strain and temperature changes, for bearing diagnostics. Due to its small dimensions, this sensor can be embedded close to, or even inside the bearing, suggesting a possible solution to the two difficulties which were discussed above.

The results of this study open new options to monitor and detect early failure signs in critical bearings. FBG-based diagnostics was found applicable and useful for detecting damage in bearings.

The analysis of signals measured on bearings with various

widths of spall, demonstrates the power of the FBG-based local sensing methodology. In addition, the study also aimed to understand the capabilities and limitations of FBG for wideband sensing, and the effect of different sensor attaching techniques on the signal.

1. INTRODUCTION

Condition monitoring is the process of tracking and assessing the health of critical machines, based on the detection, diagnostics and prognostics of a failure in mechanical systems, especially in rotating systems. Bearings are one of the vital elements of these systems. They are used to support moving parts and decrease the friction between rotating components. While in widespread use, bearings are prone to unexpected failures that can result in irreversible damage. Avoiding this failure in bearings can be achieved by the detection of the damage initiation. Therefore, detection, diagnostic and prognostics of damage in bearings have attracted considerable attention in the last decades. Early work on this topic (Heng, Zhang, Tan and Mathew (2009) and Sawalhi & Randall (2008).

A classical method for monitoring bearings is based on the analysis of vibrations. The vibration signal is usually captured by a sensor, such as a velocimeter or accelerometer. The difficulty in bearing monitoring is the presence of high vibrations excited by other parts in the machine, while the vibrations originating from the bearing are much weaker. Moreover, the vibration sensors are often not installed near the fault in the bearing. This decreases the capability to detect vibrations from bearing defects. The stronger and cleaner the signals, the more reliable are the estimated severity and location of the damage. Therefore,

complicated algorithms of signal processing are required for separation of sources of excitation.

We assume that closer location of the sensor to the defect in the bearing will help to overcome these problems. In this way, the recorded signal from the fault is less affected by the transmission path to the sensor and the bearing signal is emphasized because the vibrations that mask the bearing excitation (vibrations from other rotating components in the system) are decreased.

First, verification experiments were performed to demonstrate our assumption that the transmission path to the sensor and noise created by other rotating components may mask the faulty bearing signal. The results of these tests confirmed our assumption. As such, we progressed to test two alternative methods, having the potential to improve the sensing of the bearing fault: one is to use a Micro Electro-Mechanical System (MEMS) and the other is to use optical fibers.

Feasibility tests for these two methods were conducted. The first was carried out by placing a MEMS acceleration sensor on the bearing itself. The second was implemented by placing an optical fiber in the bearing housing and measuring the strain. The strain was measured by a fiber Bragg grating (FBG) sensor, whose characteristics are described by Kersey, Davis, Patrick, LeBlanc, Koo, Askins, Putnam and Friebele (1997). An implementation of basic bearing condition monitoring to of a subsea pump using FBG are presented by Jone, Staveley and Vialla(2014).

Both methods show good capability to detect the bearing faults. Each method has its advantages, discussed in the article. The results and the analysis of the experiments are presented, as well as the future steps required to develop each method.

2. THE ASSUMPTION VERIFICATION

The assumption is that placing the sensor closer to the defect would increase the capability of defect detection. The first phase was to verify our assumption by experimentation. The aim of this experiment is to compare the detection efficiency of the vibration sensors at two different locations.

The experimental system includes two components: a generic test unit and a measurement unit. The generic test unit allows the performing of experiments, including an emulation of a wide range of faults and kits. The test unit includes a variable-frequency drive that controls an electric motor. The measurement unit from National Instruments (NI) includes a data acquisition system connected to the vibration sensors and a Keyence optic sensor that allows measurement of the shaft speed, a setup that was used successfully by Kogan, Shaharabany, Itzhak, Bortman and Klein (2013).

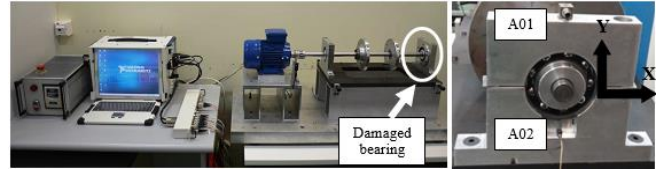


Figure 1. (a) Test system (b) Sensor locations.

The kit used in the tests contains a shaft supported by two bearings with two flywheels. The tested bearing is placed in the right bearing housing (marked at Fig. 1a). Eight different bearings were monitored, one healthy and seven faulty bearings with different fault sizes. The defects were located in the outer race in the center of the loading zone for better detection as was shown by Mendelovich, Sanders, Kogan, Battat, Klein and J Bortman, (2014).

Two piezoelectric accelerometers were installed (see Fig 1b and Table 2); a tri-axial accelerometer (3053B2 product of Dytran) on the top of the bearing housing (marked as A01) and a uniaxial accelerometer (2250A-10 product of Endevco) on the groove in the bearing housing (marked as A02).



Figure 2. Analysis procedure (PSD- power spectral density)

The data analysis procedure is described in Fig. 2. All the tests in this configuration were analyzed using the same flow chart. For a quantitative comparison of the detection capability of sensors, a figure of merit was defined as the ratio between the energy of the peaks related to the bearing and the total energy of the signal ($E_{\text{defect}}/E_{\text{total}}$).

The ball pass frequency outer ring (BPFO) for the NSK 6208 ball bearing is at 3.6 order. The data was acquired in 60 sec segments with a sampling rate of 25 kHz. The experiments included seven groove faults of various sizes and one healthy bearing, a set that was used in the early work of Mendelovich et al. (2014).

A set of experiments were performed with each bearing. The results are shown in Fig 3. For small faults, the results are not conclusive but for faults with widths above 2mm the closer sensor (A02) produce better signal to noise ratio, i.e. the Energy ratio of the closer sensor (A02) is higher than the Energy ratio of the more distant sensor (A01).

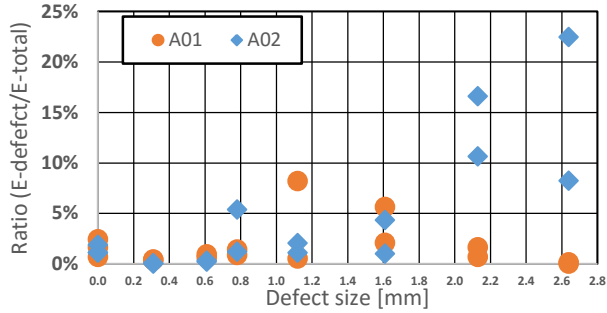


Figure 3. Energy ratio $E_{\text{defect}}/E_{\text{total}}$ vs. defect size.

3. MEMS ACCELERATION SENSOR

As assumed, the closer location of the sensor to the defect produces more effective defect detection. Therefore, a miniature sensor that can be mounted in/on the bearing was selected, i.e. a capacitive acceleration sensor based on MEMS technology. At this stage the feasibility of detection of faulty bearings using a MEMS accelerometer was tested. This sensor was mounted on the outer race of the bearing (see Fig. 4). The purpose of the experiment is to detect the defect with the MEMS sensor (marked as A03) and to compare the result with the piezoelectric sensor A01 (see Fig. 4).

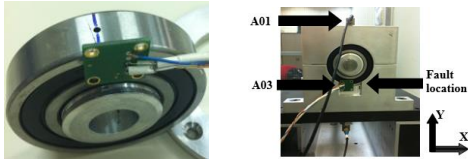


Figure 4. (a) MEMS accelerometer placed on the outer race, (b) Fault and sensor locations.

The experimental setup and the procedure are the same as described in Sec. 2; only the type of sensors and their locations are different. The MEMS sensor is a uniaxial accelerometer model ADXL001-70 produced by Analog Device (see Table 2). The same energy ratio, energy of the peaks related to the bearing fault vs. total energy, $E_{\text{defect}}/E_{\text{total}}$, was used to represent the detection capability of the sensors.

Fig. 5 shows the power spectral density (PSD) of the vibrations in the order domain. In spite of the noise level of the A03 (MEMS) sensor that can be observed in Fig. 5, the peaks of BPFO harmonics from the A03 sensor are higher compared to A01 sensor. The results of different Energy ratios are shown in Table 1. Due to the high noise level of A03 (MEMS) sensor, its total energy (E_{total}) is the highest. Despite this noise level, its energy ratio is higher, indicating that its location on the outer race is better for defect detection.

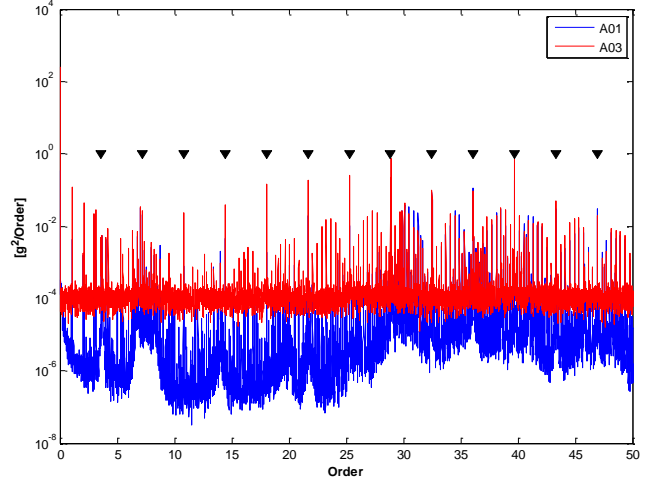


Figure 5. PSD of A01 (Dytran) and A03 (MEMS) sensors.

Table 1. Comparison of the ratio between defect energy, Unbalance energy and total energy

	E_{defect}	E_{total}	Unbalance Energy	$E_{\text{defect}}/E_{\text{total}}$	Unbalance $/E_{\text{total}}$
A01	0.101	7.831	0.068	1.29%	0.87%
A03	0.297	20.549	0.074	1.45%	0.36%

4. THE FIBER BRAGG GRATING (FBG) FIBER-OPTIC SENSOR

Here the aim was to create a bearing housing with an embedded sensor inside of it, as close as possible to the bearing. The use of standard piezoelectric accelerometers or velocimeters, MEMS technology and other traditional sensors is very difficult. Therefore, a new measurement method using an optical fiber strain gauge was chosen. Due to its small dimensions, the fiber can be embedded into various systems and structures. It allows the sensing of strain and temperature. Moreover, it has immunity to electromagnetic interference, it is electrically passive operation and of good accuracy (Gayan, Epaarachchi, Wang, and Lau, 2012).

Therefore, recently fiber-based sensing has found an increasing number of applications in structural health monitoring, replacing/augmenting other vibration sensors.

4.1. FBG sensor background

A fiber Bragg grating sensor comprises a short (a few millimeters) periodic perturbation of the refractive index along the core of a single mode optical fiber. This periodic corrugation with a period of Λ and refractive index n_{eff} , Fig. 6, selectively reflect light in a very narrowband of wavelengths around the Bragg wavelength of peak reflection, λ_0 , which is given by (Kersey et. al. (1997),

Othonos & K Kalli (1999) and Thursby, Culshaw and Staszewski (2006)):

$$\lambda_B = 2n_{eff} \Lambda \quad (1)$$

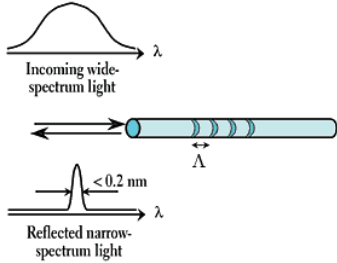


Figure 6. A FBG structure, with spectral response.

Adapted from “Acceleration/Vibration Tunable Lasers for Multichannel Fiber-Optic Sensors”, 2003

Since strain (Fig. 7) and/or temperature affect both Λ and n_{eff} , these two measurands shift the wavelength of peak reflection from an appropriately chosen reference value, λ_0 , according to:

$$\frac{\Delta\lambda}{\lambda_0} = C_\epsilon \epsilon + C_T \Delta T \quad (2)$$

where $\Delta\lambda = \lambda_i - \lambda_0$, λ_i is the shifted wavelength, C_ϵ and C_T are material constants, ϵ is the strain and ΔT is the temperature change. For germano-silicate single-mode fibers, working around 1550nm, $C_\epsilon = 0.788$ and $C_T = 8 \cdot 10^{-3} [^\circ\text{C}]$ (C_T depends on the fiber coating).

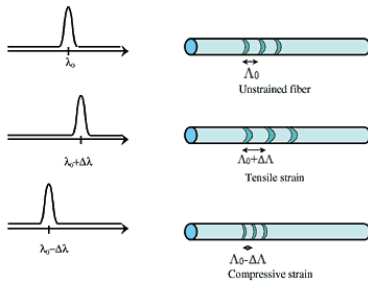


Figure 7. Spectral response under tensile strain.

Adapted from “Acceleration/Vibration Tunable Lasers for Multichannel Fiber-Optic Sensors”, 2003. (9)

The FBG sensor is easily multiplexed: Tens of FBGs, each written (via UV exposure) with a different Λ , producing multiple and different reflection peaks $\{\lambda_0\}$, can be placed on the same strand of fiber, see Fig. 8.

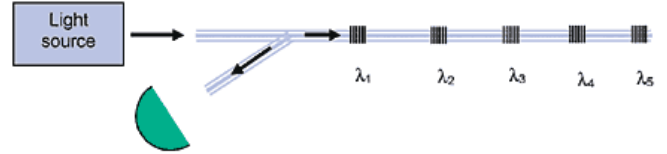


Figure 8. Multiple FBG (with different wavelengths) locations along one fiber.

Adapted from “Acceleration/Vibration Tunable Lasers for Multichannel Fiber-Optic Sensors”, 2003

The FBG interrogator used in the experiments reported here uses a tunable laser to scan some tens of nanometers around the wavelength of 1550nm. Constantly monitoring the power of the reflected light it finds and reports the locations of the peaks of the different FBGs along the fiber, provided their peak reflection wavelengths do not overlap. Proper design of those reference wavelengths, taking into account the expected spectral shifts (fairly small in these experiments), ensures proper and valid results. Comparing the measured peaks under strain with their initial values, one can calculate the induced spectral shifts and using Eq. (2) the strain can be determined. Indeed, there is also a need to monitor the temperature in case it changes throughout the experiment. However, for vibration measurements at high frequencies it is the strain and not the temperature that mostly affects the spectral shifts.

4.2. EXPERIMENTS AND RESULTS

The goal of the current experiments was to test the feasibility of bearing damage detection using the FBG optical fiber. The basic experimental setup and procedure are the same as described in Sec. 2. The FBG sensors were placed on the bearing housing (see Fig. 9) where the “Tt” and “Tb” locations measured tangential strain, on the top (180° in respect to the fault) and on the bottom (45° in respect to the fault) of the bearing, respectively, while the “R” sensor measures radial strain (45° in respect to the fault). Data were acquired in 60 sec segments with a sampling rate of 10 kHz.

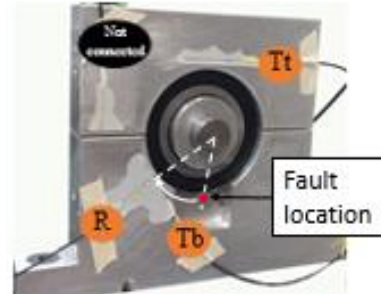


Figure 9. FBG sensors and fault locations.

Data analysis included a few steps, as shown in Fig. 10. The raw data from the optical measurement system contains time steps and wavelength peaks of the reflected light. Using Eq. (2), the data are converted into strain under the assumption

that the temperature is either constant (since the experiment takes only a short time), or, alternatively that it changes very slowly (giving rise to near DC spectral components). Then, the time domain data are transformed into the frequency and order domains for analysis.

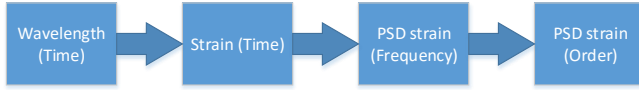


Figure 10. Analysis flow chart for optic fiber measurement

Fig. 11 presents the order spectra of the healthy and damaged bearing based on the FBG sensors. In the healthy bearing, only two harmonics of BPFO and only a few sidebands can be observed. However, in the damaged bearing there are much more (up to 10) harmonics of BPFO and more sidebands around each harmonic. It is obvious that the fault is easily detected. Moreover, it can be seen from Fig. 12, that the larger defects generate higher ratios. The analysis of signals measured on bearings with various widths of spall, demonstrates the power of the FBG-based local sensing methodology.

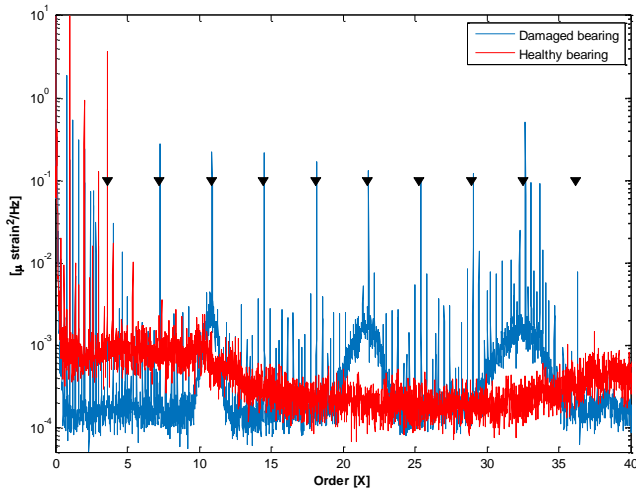


Figure 11. PSD of damaged (blue, 2.64 mm width) and healthy bearing (red). The triangles mark the BPFO harmonics.

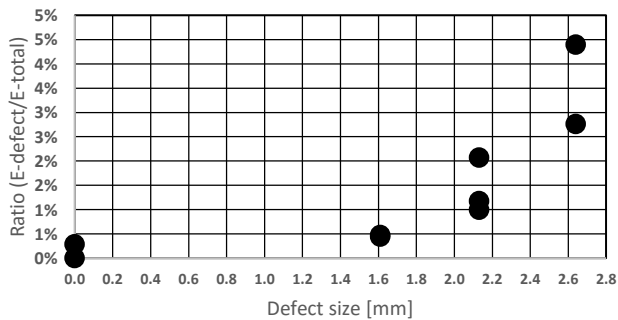


Figure 12. The ratio of $E_{\text{defect}}/E_{\text{total}}$ vs. defect size, measured by FBG (Tb) sensor

Basic tests were conducted to determine the effect of three parameters: the interrogator type, the position of the sensor relative to the impulse and the way of implementation of the FBG into the part

The implementation of FBG-based strain sensors for bearing health monitoring requires adaptation for wideband measurements including the sensing direction and mounting method.

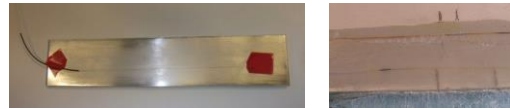


Figure 13. FBG attached to the test aluminum plate.

Tests were conducted to study the influence of different factors on wideband strain measurements. Two FBG sensors were attached to an aluminum rectangular plate (Fig. 13). The first was placed directly on the aluminum with layer of 3M DP100 clear epoxy adhesive applied above the fiber. As for the second fiber, two layers of dry Glass fabric (each 0.120 mm thick) and a generous amount of adhesive were placed between the fiber and the aluminum plate.

An impulse was generated by dropping a steel ball onto the aluminum plate. The ball (represented by an orange circle in Fig. 14) was dropped on three location: A – Short side, B – Long side and C - Perpendicular.



Figure 14. Generating impulse on 3 location on the left short side and on the right long side

The result presented in Fig. 15 indicates that similar strain spectra were produced as a result of impulses at different locations on the aluminum plate. The levels differ in the three locations but the frequency content is similar.

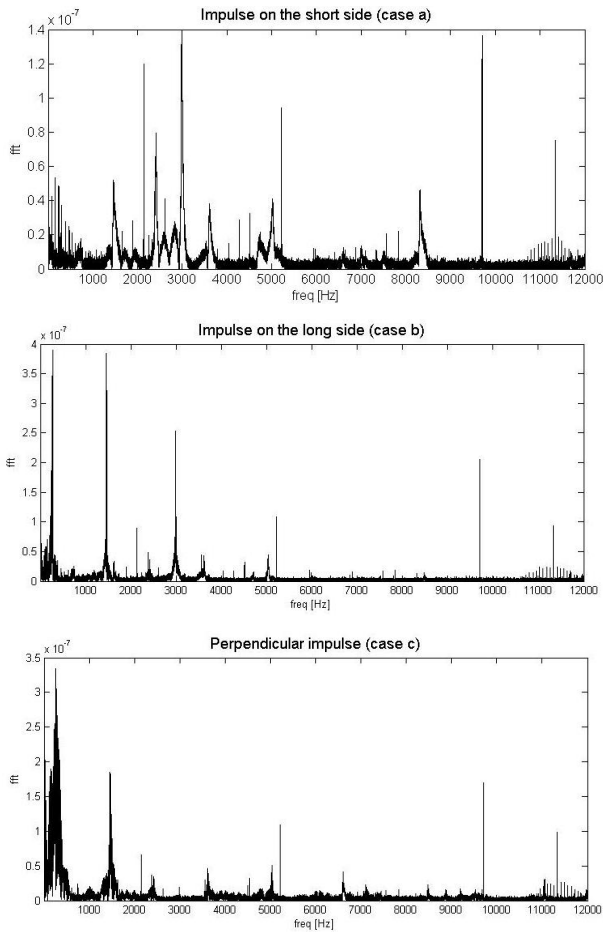


Figure 15. Power spectra of the strain as a result of impulse

Fig. 16 demonstrates the response similarity of the FBG sensors mounted on the plate using different methods of attachment (Fig. 13). Again both cases excite similar frequencies in the high range.

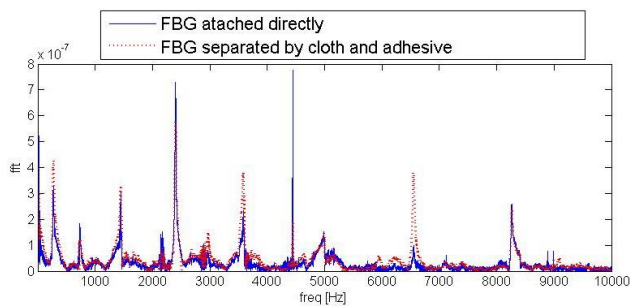


Figure 16. Comparison between two types of attachments

The two different parameters that were tested: Relative direction between the FBG and the impulse and implementation method of the show no difference in the strain power spectra.

In the next step it is planned to test different configurations of the FBG sensors mounted inside the bearing housing.

5. SUMMARY AND CONCLUSIONS

This paper presents a research for improved bearing sensing for diagnostics. By placing miniature sensors in immediate proximity of the bearing, the signal-to-noise ratio of the bearing vibrations is considerably enhanced and transmission path issues are reduced.

Two implementations were investigated: a MEMS accelerometer on the bearing outer race, and measurement of strain using an optical fiber on the bearing housing. These two methods were successfully tested for the detection of bearing faults, thereby demonstrating their promising potential. In both methods, the closer sensors provide better identification of the defects, despite the currently imperfect sensors' features.

Series of basic tests were conducted to better understand the influence of the different factors involved when designing the sensor. A similarity of the response was demonstrated for two variables that were tested.

Further improvements are planned by placing the sensors even closer. For example, multiple FBG sensors, all on the same strand of fiber, will soon be embedded in the bearing housing. In addition, a properly structured MEMS sensor can be integrated onto or even into the bearing race. Such integrated solutions are expected to provide better detection, more reliable diagnostics and improved prognostics capability of the bearing's health status.

ACKNOWLEDGEMENT

We gratefully acknowledge the invaluable support of Mr. Tal Yehoshua. We would like to thank the Perlston Foundation.

REFERENCES

M Khmelnitsky, J Bortman, U Ben-Simon, R Klein and M Tur,(2015) *Improved bearing sensing for prognostics: from vibrations to optical fibres* Insight - Non-Destructive Testing and Condition Monitoring, Vol. 57, Num. 8, August 2015, pp. 437-441(5)

A Heng, S Zhang, A C Tan and J Mathew, ‘Rotating machinery prognostics,(2009): *State of the art, challenges and opportunities*. Mechanical Systems and Signal Processing, vol. 23, no. 3, pp. 724–739, Apr.

N Sawalhi and R B Randall,(2008), *Semi-automated bearing diagnostics – three case studies*. School of Mechanical and Manufacturing Engineering. The University of New South Wales, Sydney, Australia.

A D Kersey, M A Davis, H J Patrick, M LeBlanc, K P Koo, C G Askins, M A Putnam and E J Friebele,(1997), *Fiber Grating Sensors*, Lightwave Technology, Journal of vol. 15, no. 8, August.

K Jones, C Staveley, JF Vialla, (2014), *Condition monitoring of a subsea pump using fibre optic sensing* , 23rd International Conference on Optical Fibre Sensors, Proc. of SPIE Vol. 9157, 91579Q

G Kogan, S Shaharabany, I Itzhak, J Bortman and R Klein, (2013), *Towards Model Based Prognostics - Characterization of Fault Size in Bearings*, Annual Conference of the PHM Society.

M Mendelovich, Y Sanders, G Kogan, M Battat, R Klein and J Bortman, (2014), *Characterization of Fault Size in Bearings*, Annual Conference of the PHM Society.

K C Gayan, J Epaarachchi, H Wang, and K T Lau, (2012),*Use of FBG sensors for SHM in aerospace structures'* Photonic Sensors 2, no. 3, 203-214.

A Othonos and K Kalli.,(1999), *Fiber Bragg gratings: fundamentals and applications in telecommunications and sensing*. Artech House.

D C Betz, G Thursby, B Culshaw and W J Staszewski, (2006),*Advanced layout of a fiber Bragg grating strain gauge rosette*, Lightwave Technology, Journal of vol.24, no.2, pp.1019,1026, February.

Acceleration/Vibration Tunable Lasers for Multichannel Fiber-Optic Sensors, Sensors Online, August 1.From: <http://www.sensormag.com/sensors/acceleration-vibration/tunable-lasers-multichannel-fiber-optic-sensors-823>

APPENDIX

Table 2. Index, type and location of accelerometers.

	Sensor	Type	Location
A01	Dytran 3053B2	Piezoelectric	Top of the bearing housing
A02	Endevco 2250A-10	Piezoelectric	On groove in the bearing housing (close to bearing)
A03	Analog Device ADXL001-70	MEMS capacitive	On the outer race of the bearing